SAND2022-15985C

# Supervisory On-line Optimal Control of an Electric Power Microgrid Design for Lunar Habitation

Joseph Young *
*OptimoJoe, Houston, TX, 77254*

David G. Wilson †
*Sandia National Laboratories, Albuquerque, NM*

Marvin Cook ‡
*Sandia National Laboratories, Albuquerque, NM*

Wayne Weaver §
*Michigan Technological University, Houghton, MI*

Marc A. Carbone ¶
*NASA Glenn Research Center, Cleveland, OH*

Jeffrey T. Csank ‖
*NASA Glenn Research Center, Cleveland, OH*

Jack Flicker **
*Sandia National Laboratories, Albuquerque, NM*

**The following article describes an optimal control algorithm for the operation and study of an electric microgrid designed to power a lunar habitat. A photovoltaic (PV) generator powers the habitat and the presence of predictable lunar eclipses necessitates a system to prioritize and control loads within the microgrid. The algorithm consists of a reduced order model (ROM) that describes the microgrid, a discretization of the equations that result from the ROM, and an optimization formulation that controls the microgrid's behavior. In order to validate this approach, the paper presents results from simulation based on lunar eclipse information and a schedule of intended loads.**

## I. Introduction

The National Aeronautics and Space Administration (NASA) has a sustained interest in developing a permanent lunar human presence with surface operations capabilities through the Artemis program [1, 2]. These missions will span multiple phases as part of NASAs framework to build a flexible, reusable, and sustainable infrastructure of increasing complexity [3]. Requirements within the Artemis missions, such as the Gateway, include the capability for autonomous operations, independent of ground operations [4]. The need for autonomy is driven by the need for increased reliability during periods of communication delays and losses. Similar requirements may be applied toward the Artemis lunar base camp.

For a lunar-based mission the outpost will need to be able to operate autonomously with minimum interactions and communications from ground-based mission controls. One of the lunar-based subsystems that will require autonomous operations is the electrical power system [5]. All aspects of a power/energy management system will need to include: power generation, energy storage systems capable of supporting eclipse ride-through cycles, and a distribution system

*Chief Scientist, Email: joe@optimojoe.com
†DMTS, Electrical Science and Experiments
‡PMTS, Systems Research, Analysis, and Applications
§Professor, Mechanical Engineering
¶Computer Engineer, Power Management and Distribution Branch
‖Computer Engineer, Power Management and Distribution Branch
**PMTS, Power Electronics and Energy Conversion Systems

to support various mission critical loads. This will encompass critical life support systems. As a first step, in realizing a power/energy management system, a preliminary supervisory on-line optimal control design is investigated as part of scheduling/planning for mission objectives associated with the lunar electric power systems application.

An on-line optimal control is also known as a model predictive control (MPC). In this kind of control, the control process is formulated as an optimization problem on a finite time horizon. The system dynamics can be implicitly represented or explicitly enforced as constraints, bounds can be added to either the control or state variables, and the overall behavior can be tuned through the modification of an objective function.

When designing the optimal control for a power system, certain features are desirable. First, it can be advantageous to allow the state and control variables to operate at different time scales. Often, a state variable such as a bus voltage will change faster than a control can be updated due to an external input or change in the control itself. Understanding and controlling these transients can be important to the safe and efficient operation of the system. Second, bounds on both the state and controls become important. Certainly, the system may require a bound on a control such as a duty cycle to be realizable, but it also likely requires a bound on a state such as the maximum energy in an energy storage device. Further, it becomes not only important to bound a state variable directly, but also its higher order derivatives. For example, it may be necessary to bound the ramp rate on how quickly a storage device can charge or discharge. Alternatively, it may be required to bound the second derivative of a bus voltage in order to limit how quickly it rings in the presence of a change in load.

In pursuit of these goals, this paper utilizes a continuous time, nonlinear model predictive control. In order to support varying time scales, the algorithm allows for different model fidelities between the state and control variables. In order to constrain the behavior of the system, the algorithm allows for both constant and nonlinear bounds on both the state and control variables as well as their high-order derivatives. Further, these bounds hold for the entire time horizon and not just at a discrete set of points. This provides additional certainty that a bound is respected between the controller's sample time.

To be sure, many software packages implement nonlinear model predictive controls. For example, MathWorks offers the Model Predictive Control Toolbox [6]. The approach in this paper differs from this toolbox in the discretization. The MPC Toolbox discretizes its nonlinear MPCs in time using an implicit trapezoidal rule or Tustin's method, which produces a discrete time control. As a result, the state and control variables operate at the same time fidelity. Further, bounds on these quantities can only be enforced at the sample points. Alternatively, GPOPS-II [7] implements a continuous time MPC based on a collocation method. This approach is similar to this paper in that they both produce a continuous time control, utilize a collocation method, and support adaptive mesh refinement. They differ in the kinds of polynomials used internally as well as their collocation points. As a result, the bounds in GPOPS-II are only enforced at the collocation points rather than over the entire domain.

In order to achieve this goal of a constrained, optimal control there has been a gradual and steady improvement in the algorithms that model these kinds of power electronics models. Wilson et al. [8] used a combined Hamiltonian and optimal control approach to the operation of a generic DC microgrid. This approach was enhanced to longer time horizons and a hybrid AC and DC microgrid in [9, 10]. In terms of the constraints, these formulations bounded the dynamics and control, but only at the discretization points. This restriction was improved by Young, Wilson, and Cook [11] who used an improved version of the algorithm to find the optimal control to an electric ship. Here, the discretization was improved to give more accurate solutions as well as bounds over the entire domain. Subsequently, this approach was also used to control microgrids powered by solar arrays [12] and wind turbines [13]. Although this approach was successful, the discretization limited the formulation to first order differential algebraic equations (DAEs) and bounds on the function and its first derivative. In response, Young, Wilson, Weaver, and Robinett [14] improved the approach to discretize a DAE of arbitrary order and allow for higher order bounds. This technique was later used in the cooperative control of wind turbines in [15].

This paper improves upon the results in [12] by applying a more powerful algorithm to the control of a microgrid powered by solar arrays. It also addresses the unique environment found on the moon where periodic, but predictable eclipses require the control to consider and prioritize how power should be used.

## II. Model

This paper models a small lunar power system consisting of three connected microgrids, a solar array and two habitat modules. Each of the microgrids contains a power deliver unit (PDU) that models the mission loads on each module. In addition, each microgrid contains a generic storage device on each of the power delivery buses. The overall topology of this microgrid can be seen in fig. 1.

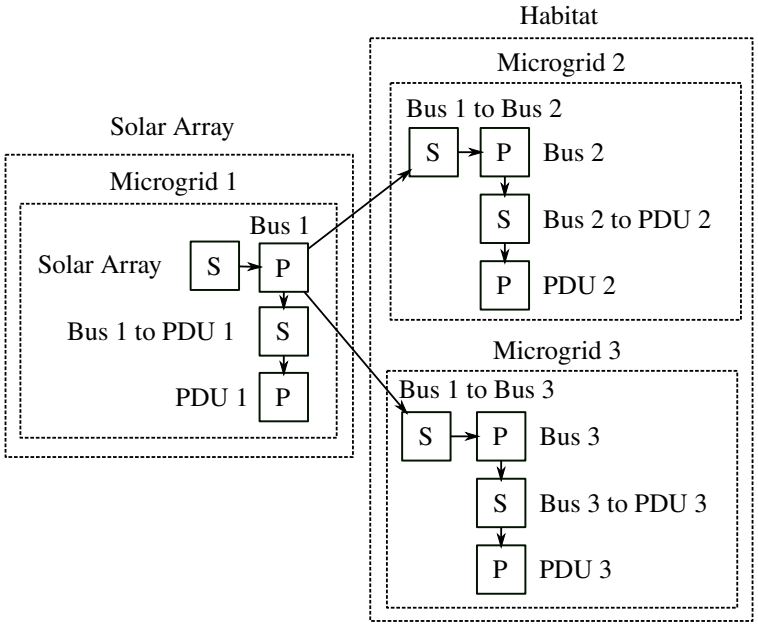


**Fig. 1 Reduced order model of the lunar habitat. P denotes a parallel DC component and S a series. Base of the arrow denotes a source and the point a sink.**

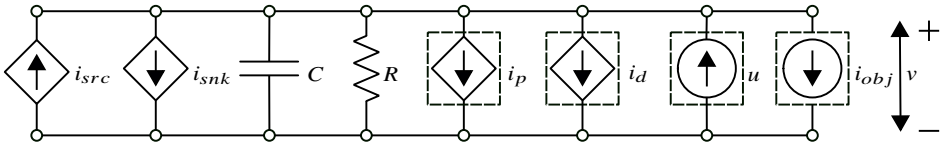


**Fig. 2 Parallel DC component used to model a DC bus**

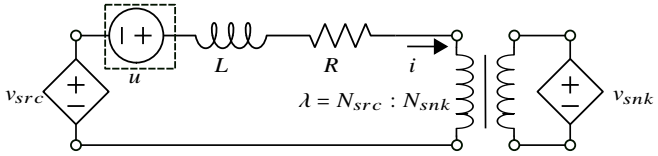


**Fig. 3 Series DC component used to model a connection between two different DC buses or model a PV array**

In order to model each microgrid, two different kinds of power system components are required and described by the circuits in figs. 2 and 3. In these diagrams, the dotted boxes represent optional components that may or may not be present due to the configuration. First, fig. 2 can represent either a DC bus that receives and delivers power to other components or acts as a device that coordinates various mission loads. Required mission loads are represented as the controlled source $i_p$ and dispatchable mission loads are represented as the controlled source $i_d$. As for energy storage, $u$ models an energy storage device connected to the bus. Its maximum amount of storage, charge, and discharge rates are modeled and bounded separately. Second, fig. 3 models either the PV array or the connection between two different DC buses. When used as a connection, the ideal transformer on the connection with voltage ratio $\lambda$ enables the two different DC buses to operate at different voltages. When used to model a PV array, voltage $v_{src}$ is set to a constant and the current $i$ is bounded in a way where it doesn't exceed the maximum amount of generation available.

In addition to the dynamics modeled as circuits, each state or control variable may contain an initial condition, bound, or a multiplicative linkage. Further, each of these additional conditions may be placed on the variable itself or on its derivative. Generally speaking, these conditions are used to add additional model information to the dynamics that are not explicitly made available in the circuit-based ROM. For example, in order to limit the maximum amount of energy stored in an energy storage device, the bound $0 \leq w \leq w_{max}$ can be added. In order to set the initial amount of energy storage, the initial condition $w(0) = w_0$ can be used. Finally, in order to coordinate two different energy storage devices, so that one does not charge another, two constraints can be multiplied and bounded such as $u = u_1 u_2$ and $u \geq 0$. This ensures that the variables share the same sign.

The dynamics for these models can be found in the following set of equations. In short, the microgrid is represented as a DAE subject to a variety of bounds that constrain the behavior of the system.

$$
\begin{aligned}
&\text{Parallel DC bus} && Cv' + \tfrac{v}{R} + \left[\textstyle\sum i_P\right] + \left[\textstyle\sum i_d\right] + \left[i_{obj}\right] + \textstyle\sum i_{snk} = u + \textstyle\sum \lambda i_{src} \\
&\text{Non-Dispatchable load} && v i_p = P \\
&\text{Dispatchable load} && v i_d = d \\
&\text{Dispatchable load bound} && d \geq 0 \\
\\
&\text{Series DC bus} && Li' + Ri + \lambda v_{snk} = u + v_{src} \\
&\text{Voltage ratio bound} && \lambda \geq 0 \\
\\
&\text{Parallel DC energy storage} && w' = -uv \\
&\text{Series DC energy storage} && w' = -ui \\
&\text{Energy storage bound} && w \geq 0 \\
\\
&\text{Initial condition} && v^{(k)}(0) = v_{k_0} \\
&\text{General bound} && v_{k_{\min}} \leq v^{(k)} \leq v_{k_{\max}} \\
&\text{Multiplicative linkage} && v = (v_1^{(k)} - c_1)(v_2^{(k)} - c_2)
\end{aligned}
$$

In order to shape the behavior of the control, these dynamics are combined with the following objective functions, which are further weighted and summed together

$$
\begin{aligned}
&\text{Use of storage} && \sqrt{\gamma^2 + \|w - w_{target}\|^2} - \gamma \\
&\text{Dispatchable load} && \sqrt{\gamma^2 + \|d - d_{target}\|^2} - \gamma
\end{aligned}
$$

Note, these objective functions use a pseudo-Huber loss function in order to measure difference between their variable and target. They are approximately linear for values greater than $\gamma$ and approximately quadratic for values less than $\gamma$. As such, $\gamma$ represents how round the objective function appears near the origin. Generally speaking, the function decreases rapidly for values less than $\gamma$, so this value also represents a quantity where the other objectives will be prioritized when the objective's value drops below this value.

To assist in setting weight and roundness of the objective function, the model parameters use the function

$$
normc(c) = \|c\| = \left( \int_0^{48\text{h}} c^2 \right)^{1/2},
$$

which computes norm of a constant function or quantity, $c$, over the time horizon. This function is used to help normalize elements in the objective function, so that their maximum value is 1 and unitless. Then, the various objectives are prioritized by weighting each quantity by an additional $1 \times 10^{-1}$ to indicate priority. Finally, the roundness parameter for the objectives, $\gamma$, is set so that values below this number are quickly deprioritized in lieu of other objectives.

## III. Discretization

In order to solve the dynamics described in section II, this control uses a discretization method developed by Young, Wilson, Weaver, and Robinett [14] and later employed in [15]. In this method, the state and control variables are discretized in the function space, akin to a finite element method, rather than in time such as with Tustin's method or a trapezoidal rule. This gives a computable method to generate a continuous control. One advantage of this approach is that the state variables can be refined independently of the control variables in order to better study, or bound, any transients that arise either from the use of the control itself or external inputs to the system. If a discrete time control is desired, the generated control can be sampled at discrete points.

More specifically, the state and control variables are each represented as a spline comprised of Bernstein polynomials, which are then satisfied at a set of collocation points defined by the Chebyshev points mapped to the divisions in the spline. The polynomials in the spline share their first and last coefficient with their neighbor, which guarantees continuity. In this way, if the spline of degree *order* contains $nele = nmesh - 1$ divisions, then the coefficients that represent the spline can be represented as a vector $c \in \mathbb{R}^{nmesh+(order-1)nele} = \mathbb{R}^{order \cdot nele+1}$.

Given this representation, the map between the coefficients and the $d$-th derivative of the spline evaluated at the collocation points can be represented as a linear operator $D^{(d)} \in \mathbb{R}^{(order-d) \cdot nele+1 \times order \cdot nele+1}$. Though, this operator assumes sufficient smoothness between the elements.

In order to guarantee smoothness between the elements, the jump in derivative is constrained to zero. In this context, jump means the difference between the derivatives of successive spline polynomials evaluated at the interior mesh points. This results in a set of linear constraints and a jumper operator of order $d$ can be represented by the map $J^{(d)} \in \mathbb{R}^{nmesh-2 \times order \cdot nele+1}$. If the DAE has degree $d$, then jump operators from 1 to $d$ are required.

In terms of boundary conditions, these conditions can be imposed directly on the spline using a process similar to that of the derivative operators. For an ODE of degree $d$, this results in a boundary condition operator, $B \in \mathbb{R}^{d \times order \cdot nele+1}$.

As an example, a first-order RC circuit governed by the equation

$$\begin{aligned} &Cv'(t) + \tfrac{v(t)}{R} = i(t), \\ &v(0) = v_0 \end{aligned} \tag{1}$$

can be discretized as

$$\begin{bmatrix} CD^{(1)} + \frac{1}{R}D^{(0)} \\ J^{(1)} \\ [1, 0, \ldots, 0] \end{bmatrix} c = \begin{bmatrix} i(t_{coll}) \\ 0 \\ v_0 \end{bmatrix} \tag{2}$$

where $t_{coll}$ are the collocation points.

In addition to the Bernstein polynomials' utility in solving DAEs, they also possess sufficient conditions for bounding a spline. Specifically, since the evaluation of a Bernstein polynomial is a convex combination of its coefficients [16], bounding the coefficients of the polynomial between $l$ and $u$ will in turn bound the polynomial itself between $l$ and $u$. This bound holds over the entire domain and not just at the mesh or collocation points. In addition, since the derivative of a Bernstein polynomial is another Bernstein polynomial, higher-order derivatives can be similarly bounded. In other words, a Bernstein polynomial based spline, and its derivatives, can be bounded using linear inequality constraints. In order to model nonlinear bounds, the difference between a Bernstein polynomial and a second constant Bernstein polynomial can be bounded.

## IV. Computational Study

The following computational study considers a 48 h period during which the lunar habitat experiences a total lunar eclipse. The eclipse lasts long enough where there is not sufficient energy storage to power all desired loads, so power must be diverted to supply mission critical loads based on prioritization levels of: required, high, medium, and low. As for the power generation, the maximum amount of power available is 30 kW, which is then scaled based on a prediction of the generation capacity. For this study, the maximum generation based on a ratio of collected irradiance measurements from the moon and normalized not to exceed the 30 kW generation maximum.

As for the objective, there are six different dispatchable loads divided between the two separate PDUs that are prioritized based on high, medium, and low priorities. Note, the required loads are not dispatchable and therefore do not contain an objective function as they are always satisfied. The goal is to supply power to these dispatchable loads, if possible, based on these priorities. In addition, there are three energy storage devices that reside on the DC buses.

There is an auxiliary goal of keeping the energy storage devices at 95% full, but this is prioritized lower than supplying power to the dispatchable loads. The number 95% is used to give the energy storage system some leeway in keeping the system stable by allowing it to store or deliver power as needed.

The rest of the parameters that characterize the model are summarized in the table below.

| | | | |
|---|---|---|---|
| Solar array voltage, $v$ | 120 V | PDU capac., $C$ | 0.01 F |
| Solar array resist. , $R$ | 0.01 Ω | PDU 2 non-disp. load, $P$ | 1875 W |
| Solar array induct., $L$ | 0.001 H | PDU 3 non-disp. load, $P$ | 1875 W |
| Solar array curr., $i$ | 30 kW max | PDU 2 disp. load, $d_{target}$ | (4240,1825,1845) W, (high,medium,low)-priority |
| Bus voltage, $v$ | $v \in [114, 126]$ V, 120 V ± 5% | PDU 3 disp. load, $d_{target}$ | (4225,1820,1855) W, (high,medium,low)-priority |
| Bus resist., $R$ | 100 Ω | PDU obj. rnd., $\gamma$ | $2.08 \times 10^4$ W s, $normc(50\text{W})$ |
| Bus capac., $C$ | 0.01 F | PDU 2 obj. weight | $(5.67 \times 10^{-7}, 1.32 \times 10^{-7}, 1.30 \times 10^{-8})$ W$^{-1}$ s$^{-1}$, $\frac{(1, 1\times10^{-1}, 1\times10^{-2})}{normc(d_{target})}$ |
| Bus energy stor., $w$ | $w \in [0, 1.44 \times 10^8]$ J | | |
| Bus energy stor. targ., $w_{target}$ | $1.368 \times 10^8$ J, 95% $w_{max}$ | PDU 3 obj. weight | $(5.69 \times 10^{-7}, 1.32 \times 10^{-7}, 1.30 \times 10^{-8})$ W$^{-1}$ s$^{-1}$, $\frac{(1, 1\times10^{-1}, 1\times10^{-2})}{normc(d_{target})}$ |
| Bus energy obj. rnd., $\gamma$ | $4.16 \times 10^7$ J s, $normc(1 \times 10^5\text{J})$ | Connection induct., $L$ | 0.001 H |
| Bus energy obj. weight | $1.67 \times 10^{-14}$ J$^{-1}$ s$^{-1}$, $\frac{1\times10^{-3}}{normc(w_{max})}$ | Connection resist. , $R$ | 0.01 Ω |
| | | Time window | 330-378 h |
| PDU voltage, $v$ | $v \in [114, 126]$ V, 120 V ± 5% | Coord. storage (Bus 1,2) | $u_1 u_2 \geq$ -5 A$^2$ |
| PDU resist., $R$ | 100 Ω | Coord. storage (Bus 1,3) | $u_1 u_3 \geq$ -5 A$^2$ |

The resulting optimization formulation contains 34 218 variables, 12 013 equality constraints, and 20 018 bounds and is solved using a prototype version of Optizelle [17]. This algorithm implements a modified version of the composite step SQP method developed by Ridzal and Heinkenschloss [18–20] combined with a primal-dual interior point method in a manner similar to NITRO described by Byrd, Hribar, and Nocedal [21]. The linear systems produced by this formulation are solved using a rank-revealing QR factorization developed by Davis [22].

Based on these parameters, the amount of power generated, along with the maximum generation capacity of the PV array can be seen in fig. 4. Here, the amount of power drawn goes to zero during the eclipse and then increases after the eclipse as additional power is needed for recharging the energy storage devices. Next, the voltage on each of the DC buses and PDUs can be seen in fig. 5. This demonstrates the control never violates the state constraint that the bus voltages remain bounded. As far as loads, the desired and actual power to four different priority loads can be seen in fig. 6. This diagram demonstrates that the control prioritizes higher priority loads over lower. Further, power delivered to required loads is never diminished, which is important for certain mission critical loads such as life support. In terms of the energy storage devices, the amount of energy found within the device is seen in fig. 7 and the power delivered is found in fig. 8. This demonstrates that control coordinates the energy storage devices to deliver power to the system for as long as possible during the eclipse. Further, it shows that each energy storage device is coordinated, so that one does not charge another.

## V. Summary and Future Work

The preceding paper provided a high level overview of an optimal control algorithm designed to safely and efficiently operate a small scale electrical microgrid that models a lunar habitat. While this environment provides some unique challenges such as periodic lunar eclipses as well as prioritized loads, the control can effectively accommodate these difficulties.

While the above methodology does not produce a real-time control, it is well-suited for a variety of use cases. For example, when integrated with a feedback control, the optimal control can provide set points for the feedback controller to follow. Alternatively, the optimal control can assist in the design of the overall microgrid. For example, the above computational study demonstrated that sufficient energy storage was not available during the eclipse to power all desired loads. Prioritization was required. Therefore, the above algorithm provides a method for testing the behavior of the microgrid given various amounts of energy storage, microgrid topologies, or other design considerations.

As for future work, additional topologies, parameterizations, and scenarios for a lunar microgrid can be considered. In addition, the integration with a feedback controller can be further explored.

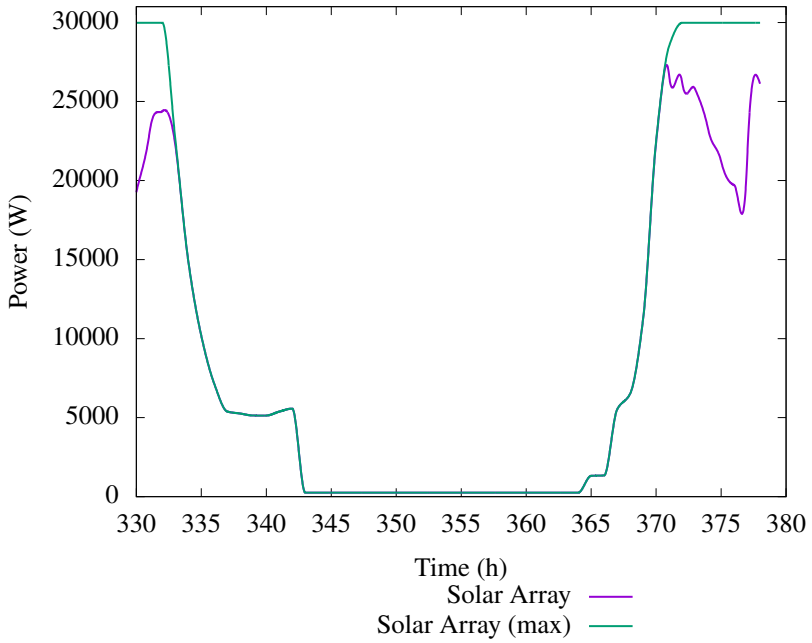


**Fig. 4 Generation by the PV array. Prior to the eclipse, the control draws additional power from the arrays to maximize the amount of power stored in the energy storage device.**

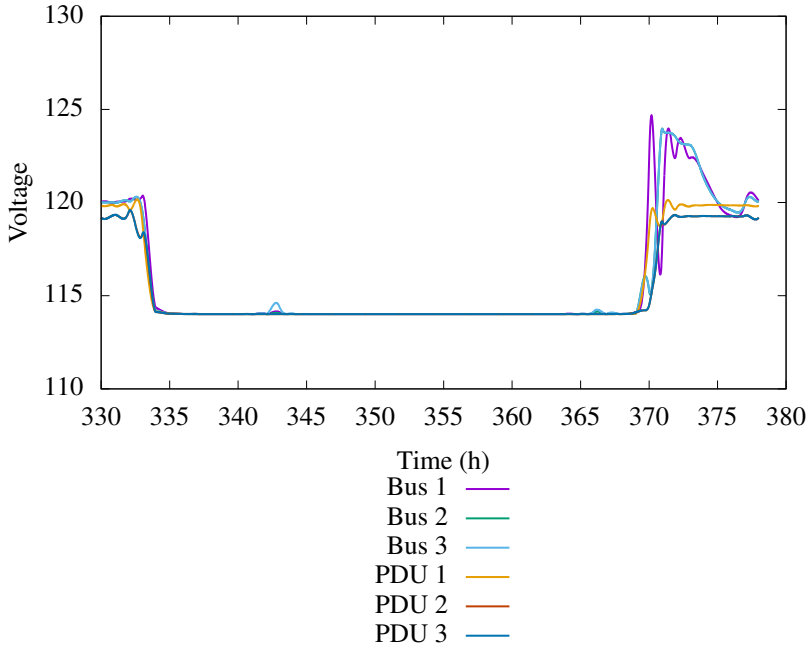


**Fig. 5 Voltage on the DC buses and PDUs. Each voltage remains within 120 V ± 5%.**

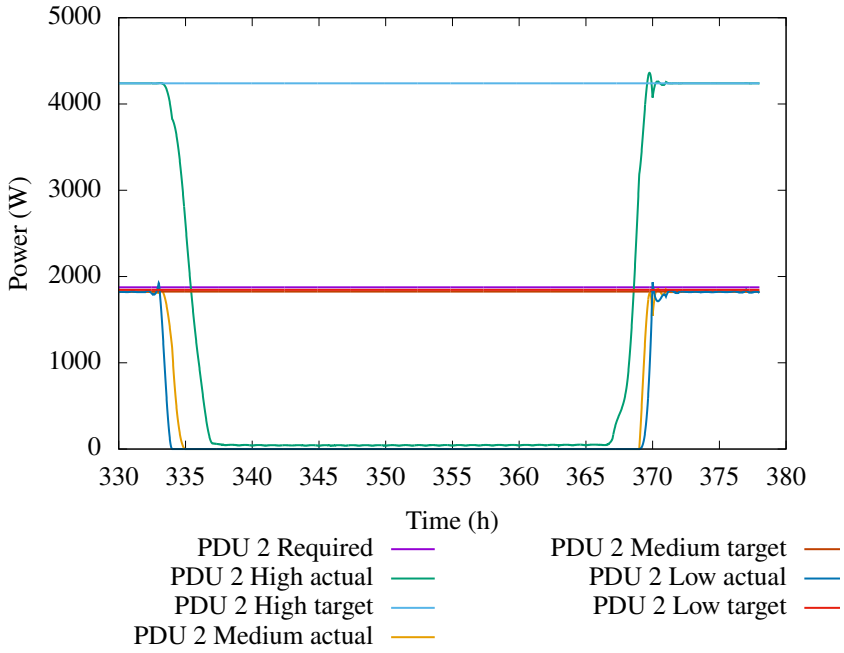


**Fig. 6 Dispatchable and non-dispatchable loads on PDU 2. Notice that lower priority loads are turned off prior to higher priority and required loads never lose power. When generation resumes, priority of loads is also respected.**

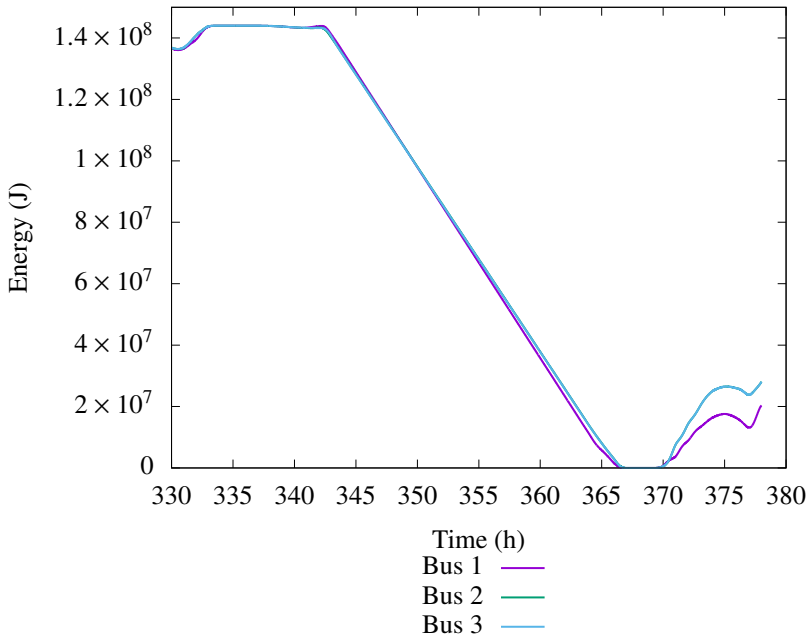


**Fig. 7 Energy in the energy storage devices. The control determines the precise time to maximize the amount storage as well as the rate to discharge.**

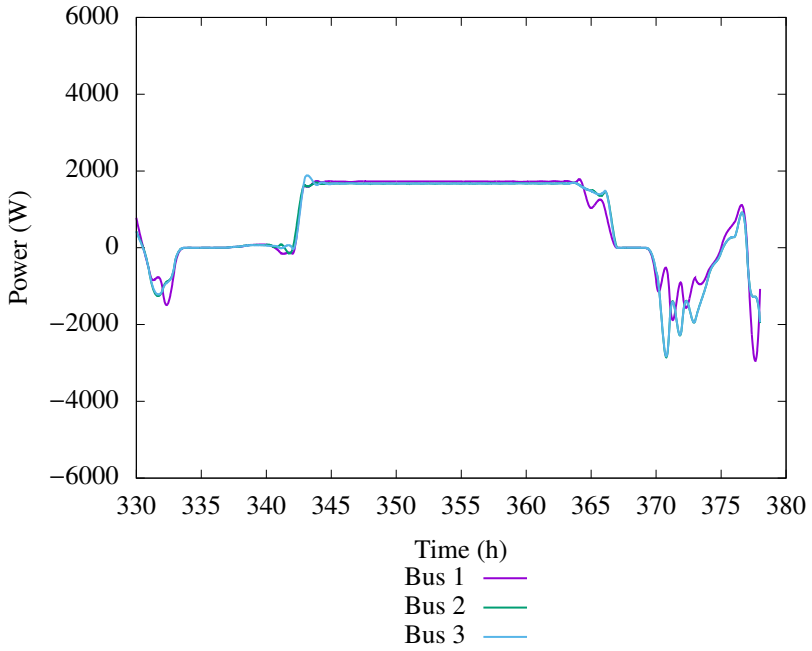


**Fig. 8 Power delivered by the energy storage devices. Here, negative power means that energy storage is charging and positive power represents discharge.**

## Acknowledgment

This article has been authored by an employee of National Technology Engineering Solutions of Sandia, LLC under Contract No. DE-NA0003525 with the U.S. Department of Energy (DOE). The employee owns all right, title and interest in and to the article and is solely responsible for its contents. The United States Government retains and the publisher, by accepting the article for publication, acknowledges that the United States Government retains a non-exclusive, paid-up, irrevocable, world-wide license to publish or reproduce the published form of this article or allow others to do so, for United States Government purposes. The DOE will provide public access to these results of federally sponsored research in accordance with the DOE Public Access Plan `https://www.energy.gov/downloads/doe-public-access-plan`.

## References

[1] Smith, M., Craig, D., Herrmann, N., Mahoney, E., Krezel, J., McIntyre, N., and Goodliff, K., "The Artemis Program: An Overview of NASA's Activities to Return Humans to the Moon," *2020 IEEE Aerospace Conference*, 2020, pp. 1–10.

[2] Creech, S., Guidi, J., and Elburn, D., "Artemis: An Overview of NASA's Activities to Return Humans to the Moon," *2022 IEEE Aerospace Conference (AERO)*, 2022, pp. 1–7.

[3] Aaseng, G. B., Frank, J. D., Iatauro, M., Knight, C., Levinson, R., Scott, J. O. M., Sweet, A., Csank, J., Soeder, J., Carrejo, D., Loveless, A. T., Ngo, T., and Greenwood, Z., "Development and Testing of a Vehicle Management System for Autonomous Spacecraft Habitat Operations," *2018 AIAA SPACE and Astronautics Forum and Exposition*, 2018.

[4] Adamek, C., "Gateway System Requirements," Tech. Rep. JSC-E-DAA-TN71173, NASA, 2019.

[5] Csank, J. T., Soeder, J. F., Carbone, M. A., Granger, M. G., Tomko, B. J., Muscatello, M. J., and Follo, J. C., "A Control Framework for Autonomous Smart Grids for Space Power Applications," *70th International Astronautical Congress (IAC)*, 2019.

[6] The MathWorks Inc., "Model Predictive Control Toolbox," `https://www.mathworks.com/products/model-predictive-control.html`, 2022.

[7] Patterson, M. A., and Rao, A. V., "GPOPS-II: A MATLAB Software for Solving Multiple-Phase Optimal Control Problems Using Hp-Adaptive Gaussian Quadrature Collocation Methods and Sparse Nonlinear Programming," *ACM Trans. Math. Softw.*, Vol. 41, No. 1, 2014.

[8] Wilson, D. G., Neely, J. C., Cook, M. A., Glover, S. F., Young, J., and Robinett, R. D., "Hamiltonian control design for DC microgrids with stochastic sources and loads with applications," *2014 International Symposium on Power Electronics, Electrical Drives, Automation and Motion*, 2014, pp. 1264–1271.

[9] Wilson, D. G., Robinett, R. D., Weaver, W. W., Byrne, R. H., and Young, J., "Nonlinear Power Flow Control design of high penetration renewable sources for AC inverter based microgrids," *2016 International Symposium on Power Electronics, Electrical Drives, Automation and Motion (SPEEDAM)*, 2016, pp. 701–708.

[10] Wilson, D. G., Weaver, W., Robinett, R. D., Young, J., Glover, S. F., Cook, M. A., Markle, S., and McCoy, T. J., "Nonlinear Power Flow Control Design Methodology for Navy Electric Ship Microgrid Energy Storage Requirements," *14th International Naval Engineering Conference & Exhibition*, 2018, pp. 1–15.

[11] Young, J., Wilson, D. G., and Cook, M. A., "The Optimal Control of an Electric Warship Driven by an Operational Vignette," *2021 IEEE Electric Ship Technologies Symposium (ESTS)*, 2021, pp. 1–8.

[12] Young, J., Wilson, D. G., Weaver, W., and Robinett, R. D., "Supervisory optimal control for photovoltaics connected to an electric power grid," *IET Conference Proceedings*, 2021, pp. 115–122(7).

[13] Young, J., Wilson, D. G., Weaver, W., and Robinett, R. D., "The Optimal Control of Type-4 Wind Turbines Connected to an Electric Microgrid," *IET Conference Proceedings*, 2021, pp. 283–290(7).

[14] Young, J., Wilson, D. G., Weaver, W., and III, R. D. R., "A Well-Conditioned Collocation Method for Optimal Control," Submitted, 2022.

[15] Young, J., Wilson, D. G., Weaver, W., and III, R. D. R., "The Optimal Control with Implicit Phase Coordination of a Collective of Wind Turbines," Accepted for publication, 2022.

[16] Prautzsch, H., Boehm, W., and Paluszny, M., *Bézier and B-Spline Techniques*, Springer, 2002.

[17] Young, J., "Optizelle – An Open Source Software Library Designed To Solve General Purpose Nonlinear Optimization Problems," `www.optimojoe.com`, 2013–2022.

[18] Ridzal, D., "Trust-Region SQP Methods with Inexact Linear System Solves for Large-Scale Optimization," Ph.D. thesis, Rice University, 2006.

[19] Ridzal, D., Aguiló, M., and Heinkenschloss, M., "Numerical study of matrix-free trust-region SQP method for equality constrained optimization," Tech. Rep. SAND2011-9346, Sandia National Laboratories, 2011.

[20] Heinkenschloss, M., and Ridzal, D., "A Matrix-Free Trust-Region SQP Method for Equality Constrained Optimization," *SIAM Journal on Optimization*, Vol. 24, No. 3, 2014, pp. 1507–1541.

[21] Byrd, R. H., Hribar, M. E., and Nocedal, J., "An Interior Point Algorithm for Large-Scale Nonlinear Programming," *SIAM Journal on Optimization*, Vol. 9, No. 4, 1999, pp. 877–900.

[22] Davis, T. A., "Algorithm 915, SuiteSparseQR: Multifrontal Multithreaded Rank-Revealing Sparse QR Factorization," *ACM Trans. Math. Softw.*, Vol. 38, No. 1, 2011.